



Faculty of Science - University of Benghazi

Libyan Journal of Science & Technology

journal home page: www.sc.uob.edu.ly/pages/page/77

Seismic facies and attribute analyses of a prograding clinoform complex, northeast Sirt Basin, Libya

Muneer A. Abdalla*, Akram M. Zafir, Ayman A. Nassar

Department of Geology, Faculty of Science, Omar Al-Mukhtar University, P.O. Box 919 Al Bayda, Libya.

Highlights

- **The prograding clinoforms are bounded by a downlap surface below and by a truncational surface above.**
- **Six seismic facies show different geometries and indicate complex lithology and depositional systems.**
- **Proximal slope and distal slope are the two major depositional systems along the clinoform interval.**

ARTICLE INFO

Article history:

Received 03 August 2022

Revised 20 May 2023

Accepted 28 May 2023

Keywords:

Seismic facies, seismic attributes, carbonate slope, clinoforms, Sirt Basin, Libya

*Address of correspondence:

E-mail address: muneer.abdalla@omu.edu.ly

M. A. Abdalla

ABSTRACT

The internal geometry and depositional system of a prograding clinoform complex are investigated using integrated 3-D seismic and wireline log data from the Assamoud Field in NE Sirt Basin, Libya, through detailed seismic facies and attribute analyses. Seismic attributes have proved to be a highly effective method for the interpretation of carbonate facies. Six major seismic facies (SF) show complex lithology and depositional systems. SF1 consists of high angle, sigmoidal, continuous reflections of high amplitude clinoforms. SF2 has high angle oblique parallel semi-continuous reflections of moderate to high amplitude clinoforms. The prograding nature of SF1 and SF2 suggest carbonate progradation into the interplatform basin through downslope shedding from the platform top and margin. SF3 consists of subparallel and semi-continuous reflections of moderate amplitude located basinward of the clinoform in SF1 and SF2. SF4 shows undulated or hummocky internal configuration and discontinuous to semi-continuous of moderate amplitude reflections and was interpreted as a basin floor fan deposited on the lower slope or basin during sea-level lowstand. SF5 displays an erosive channel-shaped geometry and wavy to subparallel semi continuous reflections of moderate to high amplitude. It was interpreted as an incised valley developed on top of the clinoforms. SF6 displays broken reflections and circular features along the upper sequence boundary which are interpreted as karst features developed as a result of subaerial exposure and erosion of the upper sequence boundary. The seismic facies and attribute analysis, log facies and their stacking patterns, and the position of the facies along the platform enabled the subdivision of the clinoform complex into two different subsystems: proximal slope that contains SF1 and SF2 and consist predominantly of thick successions of limestone with a minor amount of mud, and a distal slope that contains SF3 and is comprised of thick limestone successions with more shale units compared to the proximal slope. The prograding clinoforms may have formed as a result of sea-level highstands when sediment supply outpaces the rate of creation of accommodation space. The truncational termination patterns on top of the clinoforms suggest major erosion and removal of the upper portion of the clinoforms.

1. Introduction

High-resolution 3-D seismic reflection profiles reveal the presence of extensive inclined strata in the Assamoud Field of the continental rift Sirt Basin. These inclined strata, which occurred during the middle Eocene, are shown as pulses seen on seismic profiles as distinct progradational clinoforms and are predominantly comprised of thick successions of carbonates (Abdalla and Yang, 2021). The Sirt Basin occupies an area of about 600,000 km², approximately 230,000 km² of which are potentially comprises hydrocarbon accumulations (Fig. 1A, B). The thickness of the sedimentary successions of Sirt Basin ranges from more than 6 km in the northeastern offshore Ajdabiya Trough to 1 km, south of the Sarir Trough along the Nubian Uplift (Fig. 1C; Roohi, 1996). The Sirt Basin is seen as a continental extensional rift basin, characterized by a series of platforms and deep troughs (Fig. 1B; Mouzugh and Taleb, 1981; Hallett, 2017).

Carbonate rocks in the Sirt Basin are considered as important hydrocarbon exploration targets. The major reservoir units in the Sirt Basin are carbonate with large production from the Eocene

strata, about 15% of the total reserves of the Sirt Basin (Wenneker *et al.*, 1996), but the characterization of these carbonate reservoirs is challenging because of the high inconsistency in the lateral facies distribution and rock properties. Therefore, this study utilizes seismic facies and attribute analyses in order to characterize the seismic architecture of the progradational clinoforms and interpret the depositional environment in which those clinoforms formed. The findings of this study will enhance our understanding of the reservoir heterogeneity of the Eocene carbonate successions and should improve future hydrocarbon exploration and production strategies through delineating the reservoir continuity and the lateral extent of the seal rocks.

2. Tectonic and stratigraphic setting

The study area is situated in the northeastern part of the Sirt Basin in Libya (Fig. 1A, B). The Sirt Basin lies on the north-central African Plate and was formed as a result of crustal extension, leading to repeated episodes of subsidence and faulting (Guiraud and Bosworth, 1997), after a series of tectonic events related to the split

of supercontinent Pangea (Van der Meer and Cloetingh, 1993; Baird et al. 1996; Lemnifi et al. 2015; Lemnifi et al. 2017). Basin rifting started in the Early Cretaceous, reached a peak in the Late Cretaceous, and ended in the early Eocene, resulting in a series of platforms and troughs in the basin (Fig. 1B, C; Roohi, 1996; Gras and Thusu, 1998; Ambrose, 2000). Four major episodes of subsidence were recognized in the Sirte Basin (Abadi, 2008). Episode I took place in the Early Cretaceous and resulted in the formation of the main E-W structural trend. Episode II was the most significant,

occurred during the Late Cretaceous, and formed the NW-SE structural trend (Fig. 1B). Episode III initiated in the early Paleocene and ended in the early Eocene, leading to the enhancement of the faults and associated structural development. Lastly, Episode IV started in the middle Eocene and is still presently ongoing. The first three subsidence episodes were formed due to repeated faulting related to rifting, whereas the final subsidence episode was formed by the cooling of the crust and sediment loading (Abadi, 2008).

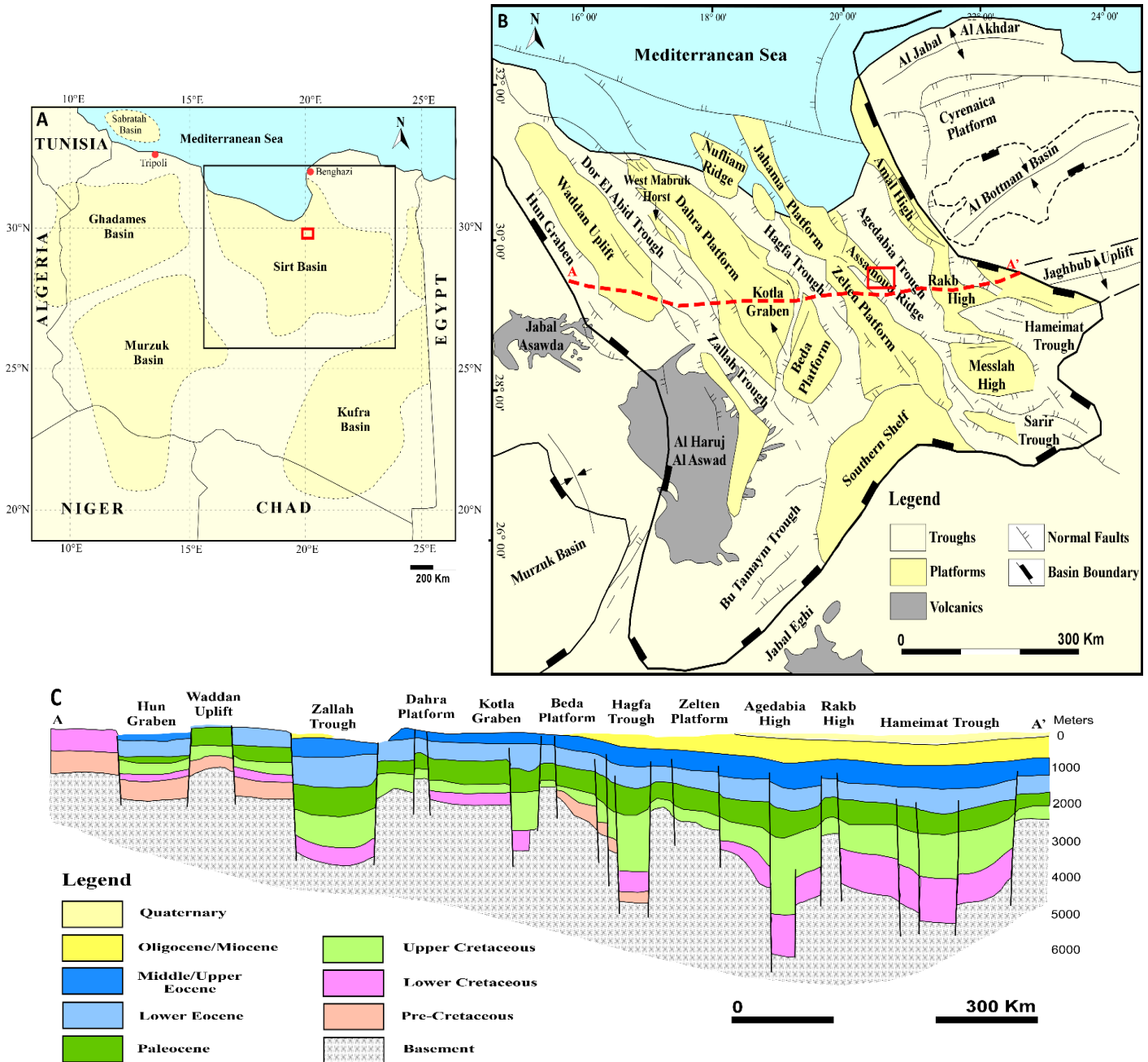


Fig.1. A) Simplified map of Libya showing the main sedimentary basins (modified after Abdalla, 2021a). B) Simple structural map of the Sirt Basin (modified after Mouzoughi and Taleb, 1981; Abadi, 2008). The basin comprises a series of horsts and grabens, and most normal faults have a NW-SE orientation. The study area is located in the northeastern part of the basin along the Assagoud Ridge, the southern extension of the Jahama Platform. Location of study area is shown by the red box. C) Structural E-W cross-section showing the major structural features across the Sirt Basin (modified after Roohi, 1996; Abdalla, 2021b). Location of the cross section is shown by the red dashed line in B. Notice that most of the normal faults associated with rifting terminate in the Lower-Middle Eocene strata, signifying that rifting may have terminated during the Lower-Middle Eocene.

The sedimentary strata of the basin range in thickness from about 1000 m in the west to about 6000 m in the east and unconformably overlie the Precambrian basement (Fig. 1C; Roohi, 1996). They consist of Cambro-Ordovician and Lower Cretaceous siliciclastic sediments deposited in the pre-rift stage, Upper Creta-

ceous-Lower Tertiary marine shale, and shallow marine carbonates deposited in the syn-rift stage. The rift deposits are unconformably overlain by the post-rift Oligocene succession which contain shallow marine sandstones (Fig. 2; Van der Meer and Cloetingh, 1993).

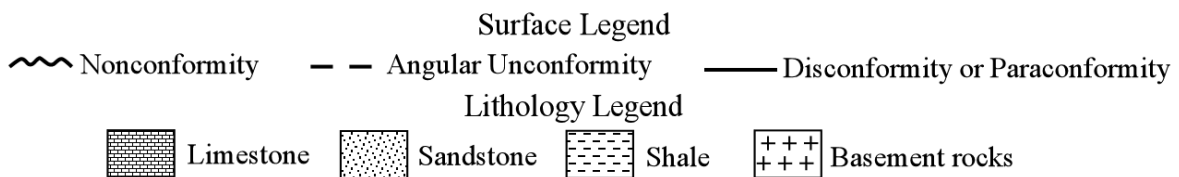
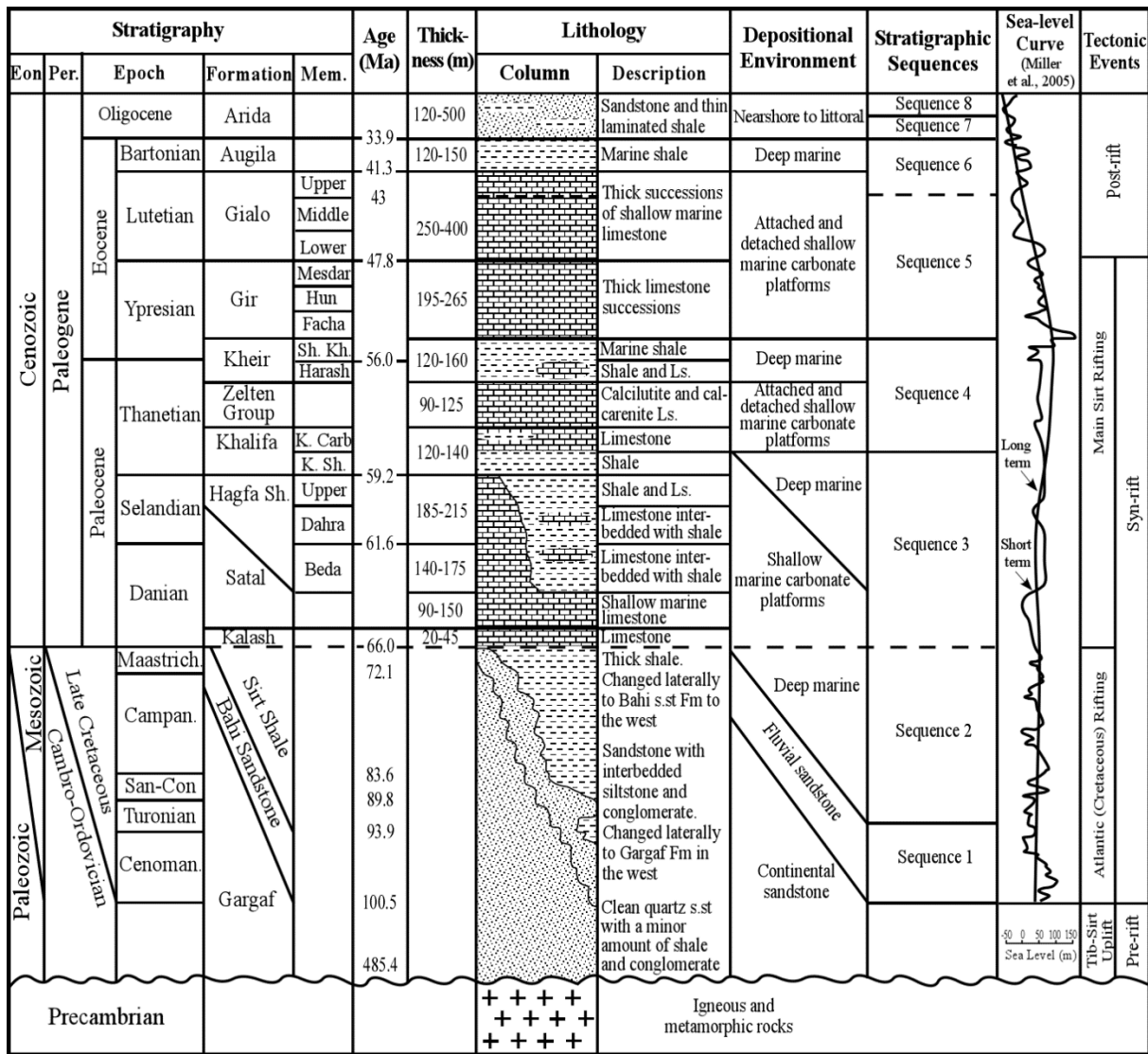


Fig. 2. Litho- and chronostratigraphy of Paleozoic, Mesozoic, and Cenozoic sedimentary successions of the study area, showing the thickness, depositional environments, stratigraphic sequences, and tectonic events (modified from El Ghouli, 1996; Abdalla and Yang, 2021). The focus interval is in the Lower and Middle members of Gialo Limestone Formation. The short and long-term global sea-level curves are from Miller et al. (2005).

3. Data and methodology

Three dimensional (3d) seismic and wireline log data were used to characterize the architecture of the prograding clinoforms. The 3-D seismic datasets cover an area of approximately 65 km², 10 km wide and 6.5 km long, and consist of 500 inlines and 480 crosslines. The maximum two-way travel time is 6000 ms, and the line spacing is 25 m. The seismic data was processed to a minimum phase and was recorded with SEG normal polarity. The frequency ranges from 8 to 60 Hz with a dominant frequency of 21 Hz. The wireline data are from three wells penetrating the clinoform interval (Fig. 3A). The wells are vertical production wells and depth was measured in measured depth (MD). The types of wireline logs include gamma ray (GR), density (RHIB), acoustic (AC), resistivity (SFLU, MSFL, ILD), caliper (CAL), and spontaneous potential (SP).

Seismic sequence stratigraphic principles of Mitchum et al. (1977) were first used to establish a time stratigraphic framework and to delineate the bounding stratigraphic surfaces of the clinoform interval. Wireline log analysis was used to interpret lithology,

stacking patterns, depositional systems, systems tracts, and stratigraphic sequences. This interpretation was carried out by Abdalla and Yang, (2021). Log facies were defined on the basis of siliciclastic mud content inferred from GR logs. They created cross plots to establish a guide between log responses and interpreted lithologies, and to interpret lithologies from wells that do not have GR logs. Synthetic seismograms were generated to tie the well interpretations to seismic data, an example is shown in Fig. 3B. The seismic facies and attribute analyses were applied in order to distinguish the main structural, stratigraphic, and sedimentological features of the clinoform interval. Seismic facies are defined as the character of a group of reflections whose seismic reflection parameters differ from those of adjacent facies units. Seismic facies analysis is the interpretation of seismic reflection parameters, such as continuity, amplitude, configuration, coherency, and frequency, within the stratigraphic framework of a depositional sequence (Sheriff, 2002).

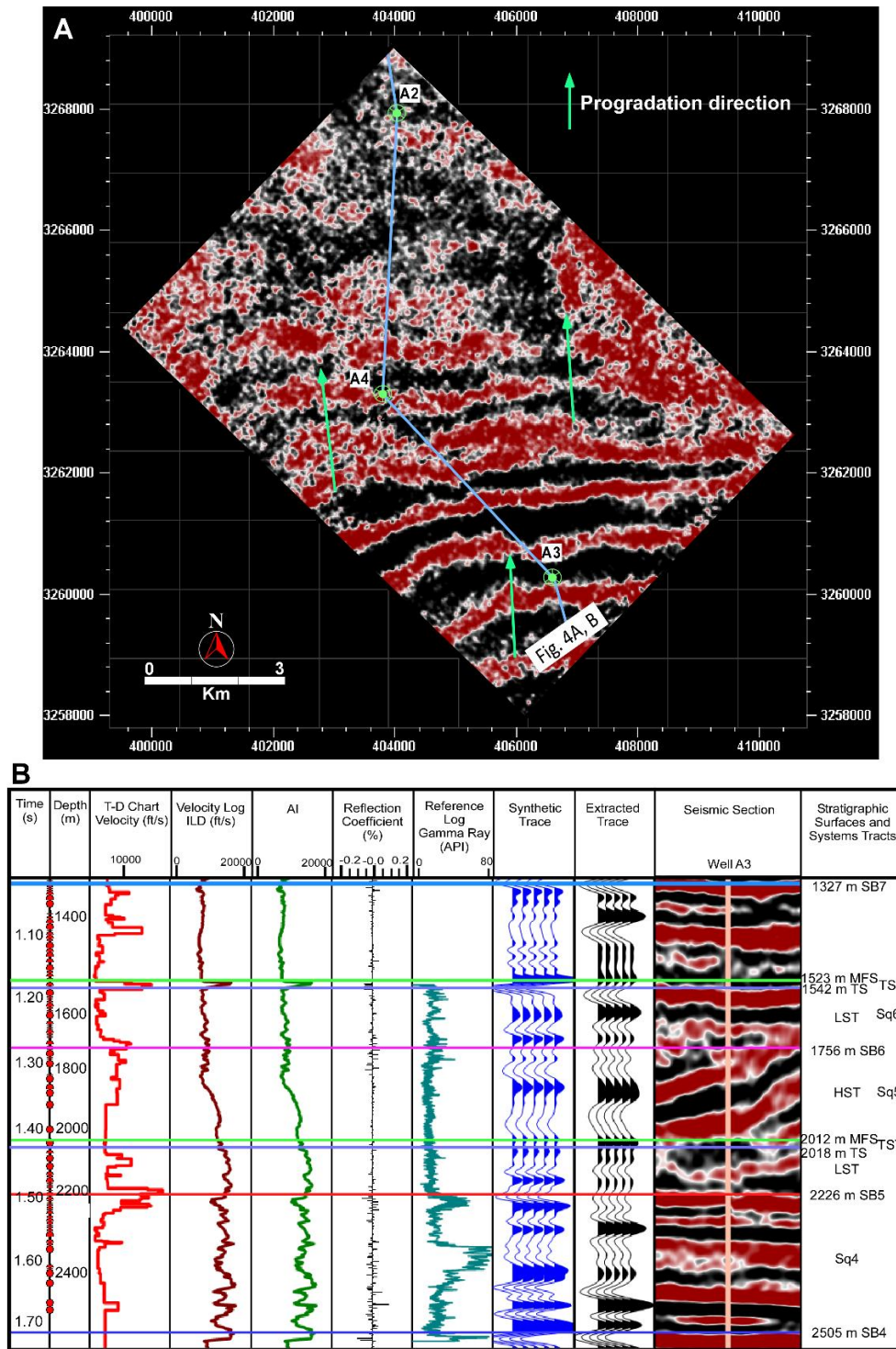


Fig. 3. A) Time slice showing the location of the three wells and progradation direction and lateral continuity of clinoforms. The clinoforms are seen as east-west linear anomalies, suggesting that the progradation direction is north and source of sediment is located in the south of study area. B) A synthetic seismogram of Well A3, showing the depth of stratigraphic surfaces and sequence stratigraphic units. SB: sequence boundary; TS: transgressive surface; MFS: maximum flooding surface; TST: transgressive systems tract; HST: highstand systems tract; LST: lowstand systems tract; T-D: time–depth; AI: acoustic impedance.

These reflections parameters are an indication of lateral lithofacies type and continuity, fluid type changes, geometry, bed thickness, and bedding patterns (Mitchum *et al.* 1977; Hart, 2012). Seismic attributes are extracted from seismic data using basic seismic measurement related to travel time, amplitude, frequency, and attenuation (Brown, 2004). Seismic attributes used in the facies characterization include instantaneous phase, local structure dip (event dip), and variance-based coherence attributes. The instantaneous phase emphasizes the lateral continuity of seismic reflections that have a great variation in amplitude. It is widely used as an indicator

of laterally continuous events, faults, pinch-outs, sequence boundaries, and reflection termination patterns (downlap, onlap, toplap, and truncation). The local structure dip or dip deviation attribute comprises an edge detection method that reveals major changes in local dip (Koson *et al.*, 2014). It is a good indicator of channels' edges and faults. The estimation of dip deviation from the seismic data uses the downslope dip method, which assumes that the gradient is perpendicular to the seismic events. The variance is a type of coherence attributes, which measures the similarity of seismic traces and their neighbors. It shows the discontinuities of seismic

reflections, and is considered as a good indicator of faults, fractures, carbonate build-up, and channel margins.

4. Results and discussions

4.1. Log facies

The Middle Eocene Gialo Formation, which contains the clinoform interval, is widespread in the Sirt Basin except in the northern part where the equivalent Gedari Formation was deposited. The Gialo Formation is mainly composed of thick successions of shallow marine limestone, dominated by large benthic foraminifera, especially nummulitids (Barr and Weegar, 1972).

Log facies were identified mainly on the basis of siliciclastic mud content interpreted from gamma ray (GR) logs. GR log values are lowest in mud-poor limestones log facies and highest in shale log facies (Fig. 4B; Abdalla and Yang, 2021). Vertically in wells A2, A3, and A4, the clinoform interval consist of 47-145 m thick coarsening upward cycles of mud-poor limestone, mud-rich limestone, and shale. In the three wells, the GR log shows coarsening upward trend or funnel-shaped pattern. Such trend displays a gradual decrease upward from maximum log readings and a gradual decrease in mud content. This log pattern is present in the entire clinoform interval, indicating a progradational stacking pattern. However, the

funnel-shaped trend in the clinoform has spikes disrupting the overall trend. These spikes may correspond to stratigraphic boundaries that divide the clinoform units into smaller parasequences or bedsets (Fig. 4B).

4.2. Seismic stratigraphy

The clinoform interval was first distinguished by the well-defined, high amplitude inclined seismic reflections on vertical seismic sections. The clinoforms extend for at least 9.5 km from south to north along a depositional dip (Fig. 4A). The vertical distance from the upper sequence boundary to the downlap surface (clinoform interval thickness/height) is ~240-330 m. The clinoform complex is well defined by truncational termination patterns at an upper sequence boundary, locally showing a channelized surface, and by a downlap relationship at a lower downlap surface (Fig. 4A). It lies on top of undulated or hummocky seismic reflectors interpreted as a basin floor fan formed during the Early Eocene (Abdalla and Yang, 2021). The clinoform interval is interpreted as a highstand systems tract of the fifth sequence of the eight sequences interpreted in the sedimentary successions of the study area (Abdalla and Yang, 2021).

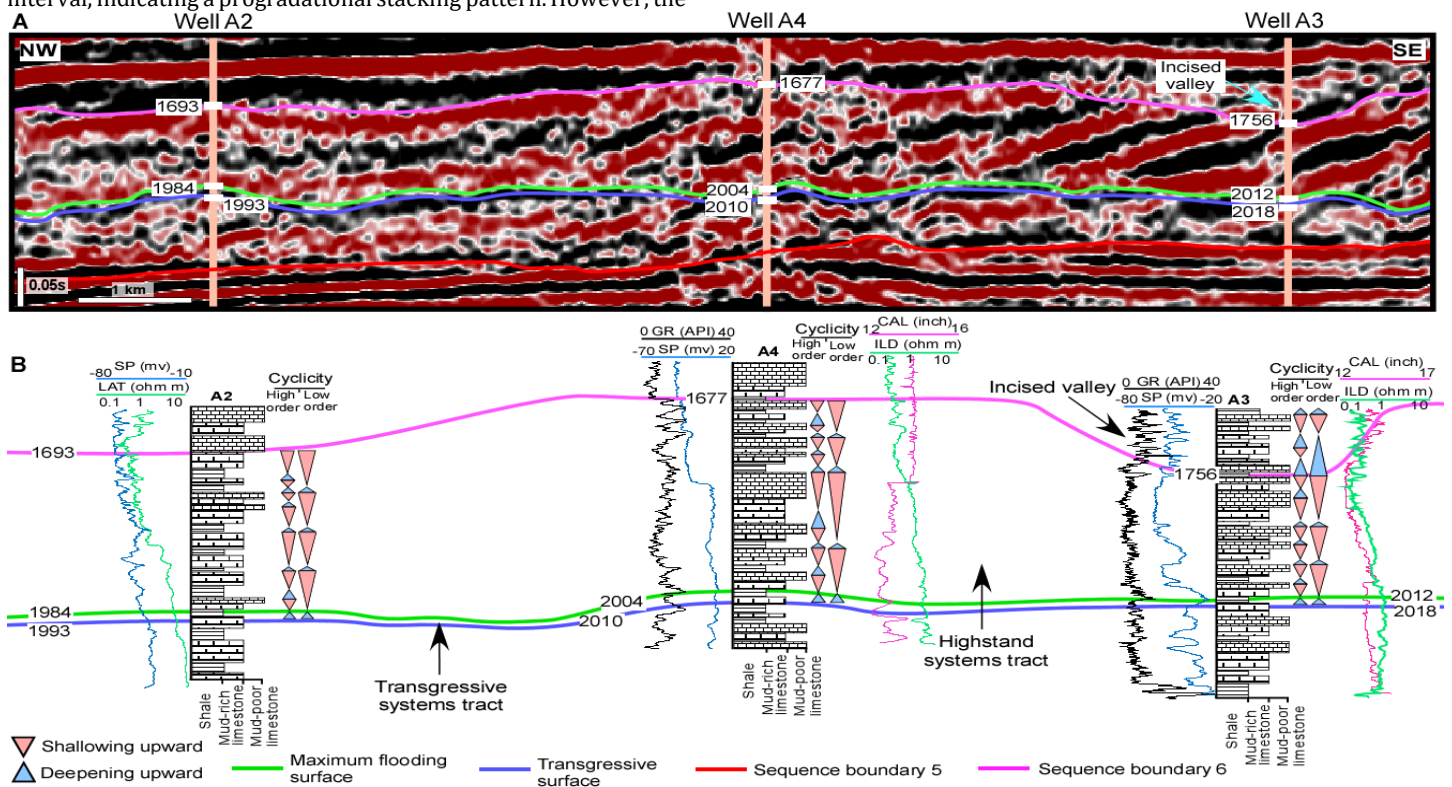


Fig. 4. A northwest-southeast seismic section along depositional dip (A) tied to wells A3, A4, and A2 showing the clinoform log facies, stacking pattern, and bounding surfaces (B). Two orders of cycles, namely high-order and low-order cycles, were defined on the basis of stacking pattern of log facies. Depth of stratigraphic surfaces is in measured depth (MD) and shown in meters on seismic and well section. See methodology section for log types.

4.3. Seismic facies and attribute analyses

Six predominant seismic facies were recognized based on the classification of Mitchum et al. (1977). The seismic facies include prograding clinoforms, subparallel/sub-horizontal reflectors at the lower part of clinoforms, hummocky or undulated bodies underneath the clinoforms, a channel-shaped body, and karst facies (Figs 5, 6, 7). Seismic attributes used in the facies characterization include the instantaneous phase, local structure dip (event dip), and variance-based coherence attributes.

4.3.1. Seismic facies 1 (SF1) and 2 (SF2): high angle prograding clinoforms

SF1 consists of a high angle sigmoidal and semi-continuous to continuous reflections of moderate to high amplitude basinward

clinoforms (Fig. 5A). The clinoforms are of high angle (19-24°) and 200-300 ms TWT high. It is characterized by truncations at the upper boundary and downlap terminations at the lower surface. SF2, which forms basinward of SF1, comprises high-angle oblique parallel clinoforms with truncation and downlap terminations (Fig. 5A). The seismic reflectors are semi-continuous to continuous of moderate to high amplitude. Similarly, to SF1, the clinoforms are of high angle (13-21°) and 200-300 ms TWT thick. The length of individual clinoforms (lateral distance from truncation to downlap) within these two facies ranges from 1.7-2.3 km. In well data, these facies consist of limestone rich successions (gamma ray log curve ranges from 5 to 20 API). SP log curves show an overall funnel-shaped trend, indicating a progradational stacking pattern (Fig.

4B). The sigmoidal and oblique parallel internal reflection configurations of SF1 and SF2 suggest carbonate progradation into the interplatform basin through downslope shedding from the platform top and margin (e.g., Hine et al. 1992). The oblique tangential reflections along the slope of carbonate platforms are speculated to develop under higher energy conditions and are composed of a grainstone or rudstone with no or very little amount of mud (Macurda, 1997). The instantaneous phase profiles clearly show truncated clinoforms at the upper surface, discontinuities along clinoforms, and chaotic reflections at the toe of clinoforms (Fig. 5B). The discontinuities are seen as elongated anomalies on variance sections and are caused by fault activities (Fig. 5D). The progressive increase in dip angle shown on the local structure dip profiles along clinoforms correlates with the discontinuities highlighted in the instantaneous phase and variance profiles suggesting the presence of sharp edges caused by faults (Fig. 5C). The highly variable dips, discontinuities, and low amplitude of chaotic reflections at the clinoform toe may indicate the presence of debris facies.

4.3.2. Seismic facies 3 (SF3): subparallel to chaotic seismic reflections

It consists of subparallel to chaotic and semi-continuous to continuous reflections of moderate to high amplitude. The thickness of this facies is ~ 200-250 ms TWT vertically and extends laterally for several kilometers and developed basinward of SF1 and SF2 (Fig. 6A). Along some seismic lines, the subparallel reflections are replaced by chaotic reflections with hummocky to chaotic internal configuration. The two prograding seismic facies (SF1 and SF2) developed on the proximal part become less inclined (nearly horizontal) at the toe of the slope, forming SF3. Seismic reflections within these seismic facies are vertically stacked and suggest that accommodation space is available vertically. This facies contains mainly limestone sediments with minor thin layers of mud represented as spikes in well logs (Fig. 4B). The position of this facies on the seismic section and its overall serrated log trend suggest lower slope deposits where sediments were transported from the platform top and margin downslope (Macurda, 1997). The instantaneous phase and variance attributes show that reflection continuity along these facies changes from moderate to low downslope as the seismic reflections change from subparallel to chaotic (Fig. 6B, C).

4.3.3. Seismic facies 4 (SF4): hummocky or undulated seismic reflections

This facies displays an undulated or hummocky internal configuration, and is discontinuous to semi-continuous of moderate amplitude reflections (Fig. 6A). Thickness of this facies ranges from ~ 80-120 ms TWT and present across the entire 3-D seismic volume. In well data, SF4 consists predominantly of limestone units interbedded with thin shale intervals. SP log curves show an overall funnel-shaped trend, indicating progradational stacking pattern (Fig. 4B). Both the instantaneous phase and the variance profiles show high discontinuities along this facies (Fig. 6B, C). SF4 is interpreted as a basin floor fan deposited on the lower slope or basin during sea-level lowstands.

4.3.4. Seismic facies 5 (SF5): channel-shaped seismic reflections

It has an erosive channel-filled shape and wavy to subparallel semi continuous reflections of moderate to high amplitude. Thickness of this facies is ~80-120 ms TWT vertically and more than 1.5 km laterally (Fig. 7A). The channel-shape feature is characterized by truncational termination patterns below indicating a subaerial exposure and erosion of lower surface and was interpreted as an incision formed on top of the clinoforms (Fig. 4A). Sediments then accumulated and filled the depression caused by erosion after a subsequent sea-level rise. The instantaneous phase section shows concave up geometry characterized by moderate to high continuity, and the high variance along the channelized surface indicates discontinuities (Fig. 7B, C).

4.3.5. Seismic facies 6 (SF6): karst facies

SF6 displays discontinuities (broken reflections) and circular features along the upper sequence boundary (Fig. 7A). It shows chaotic wave internal configuration of semi-continuous and high amplitude reflections. The instantaneous phase is highly discontinuous within this facies and the variance time slice shows high coherence circular features correlating with the irregular top surface of upper sequence boundary (Fig. 7B, C). These irregular shapes vary in diameter and are most likely produced by karstification and formation of paleocaves on the platform before its final demise.

4.4. Depositional systems

Fig. 8 is a Schematic model of the studied clinoforms during its subaerial exposure showing the interpreted depositional system based on the seismic facies and attribute analyses. According to Abdalla and Yang (2021), the prograding clinoforms developed on the leeward side of an isolated carbonate platform. The geometry, angle of inclination, height, and lateral extension over several kilometers of the limestone prograding clinoform observed on 3-D seismic profile suggest a slope depositional system (Fig. 4A). The seismic facies and attribute analysis, and the log facies and their stacking patterns enabled the subdivision of slope system into two different subsystems. The two depositional subsystems are proximal slope and distal slope, which are named on their position along the slope profile.

4.4.1. Slope depositional system

The main depositional area for sediments derived from platform top and platform margin is slopes of carbonate platforms. Pelagic and platform derived sediments falling from the water column and sediments carried by mass gravity flows are the two possible sources for slope deposits (Eberli et al. 2004). The slope morphology and declivity is controlled by several factors, including composition of sediments, rate of sedimentation, erosion on platform top and margin and ocean currents (Cook & Mullins, 1983; Kenter, 1990; Adams & Schlager, 2000). The slope of prograding clinoforms of our Eocene platform example is approximately 240-330 m high and has a maximum inclination of 24°. It consists of various seismic facies associated with different sedimentary facies and depositional process. Each of these facies is distinguished by its unique seismic facies characterization, and log curve shapes and stacking patterns. The two slope subsystems are described in detail in the following section.

4.4.1.1. Proximal slope

The prograding clinoforms of the Eocene carbonate platform vary in length. The lateral extension of the clinoforms near the platform top ranges from 1.7-2.3 km, while the nearly horizontal clinoforms at the lower slope extend for more than 6.5 km basinward. On seismic profile, the first two set of clinoforms exhibit sigmoidal and oblique parallel patterns. The seismic reflections of the clinoforms top vary in amplitude and continuity and are truncated against the upper sequence boundary. Well A3 is the shallowest well drilled on the platform and penetrated through different parts of the first set of clinoforms (SF1). The proximal slope facies consist predominantly of thick successions of limestone with a minor amount of mud. The gamma ray log of the proximal slope facies shows an overall prograding and aggrading serrated pattern (Fig. 4B). The serrated log shape reflects fluctuations in GR readings over a short interval of vertical well section. The high values of GR log display spikes, which indicate the presence of thin layers of mud within the limestone successions. Those spikes subdivide the stacked upper clinoform facies into parasequences or bedsets. The thickness of these parasequences changes systematically upward through the clinoform top from thick to thin and thick again (Fig. 4B).

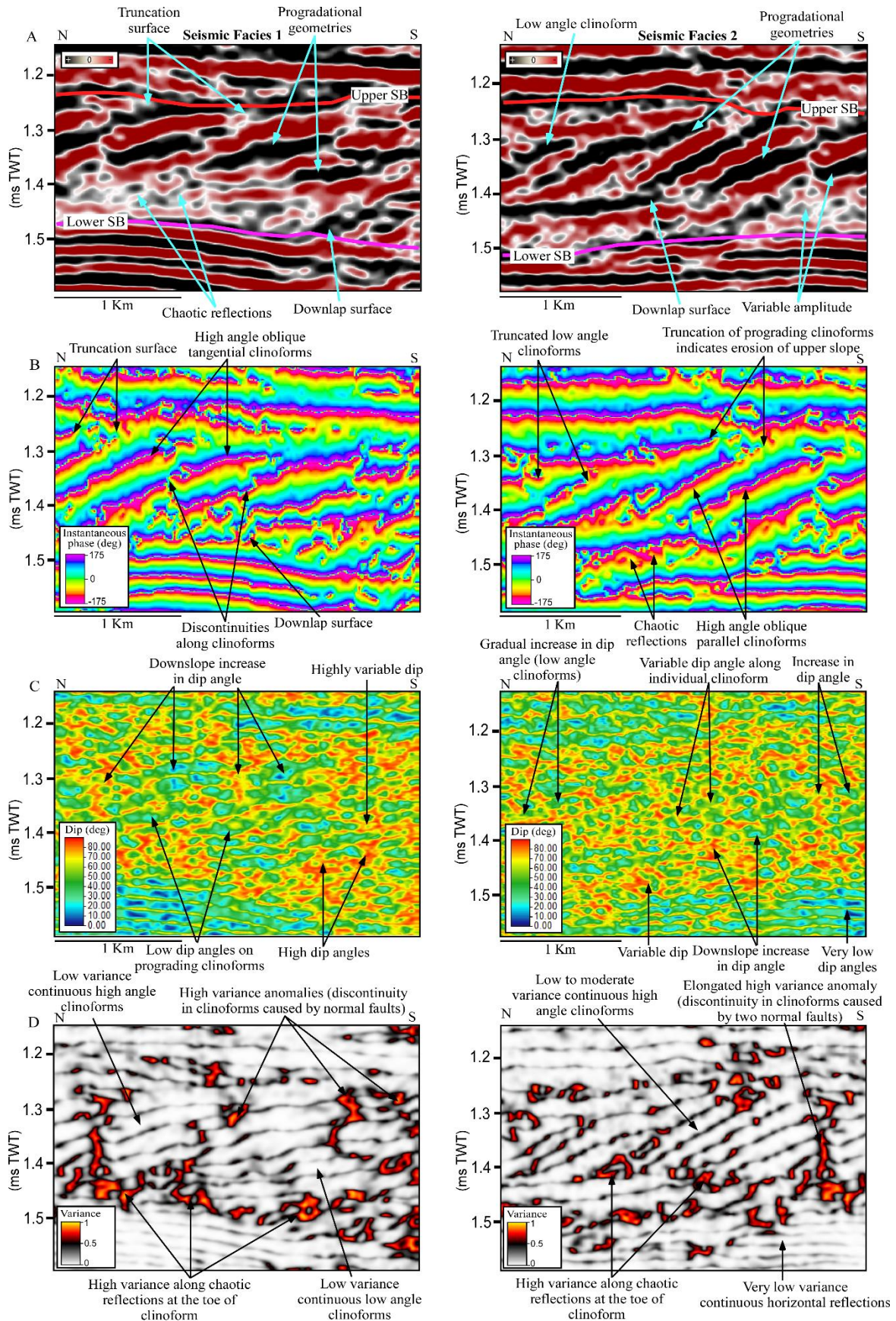


Fig. 5. A) Seismic vertical sections showing the amplitude and geometry of SF1 and SF2. The reflections show sigmoidal and oblique parallel stratal patterns. B) The instantaneous phase profiles of two facies show the lateral continuity and nature of reflection terminations against the upper and lower surfaces. C) Seismic sections highlighting the dip of SF1 and SF2. The progressive increase in dip angle shown on the local structure dip profiles along clinoforms correlates with the discontinuities highlighted in the instantaneous phase and variance profiles suggesting the presence of sharp edges caused by faults. D) Variance attribute illustrates the discontinuities along clinoforms caused by faults and chaotic reflections.

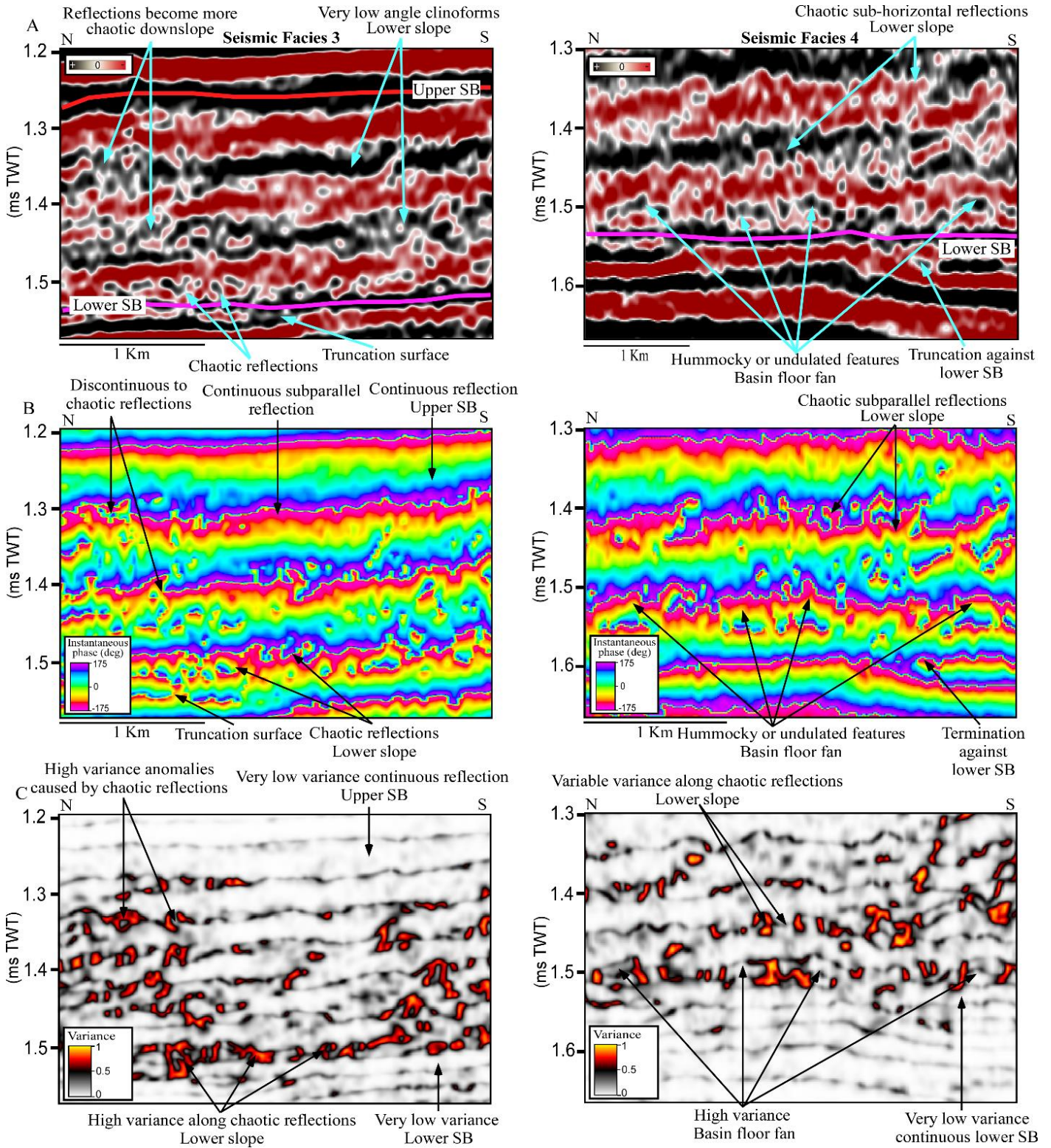


Fig.6. A) Seismic vertical sections showing the amplitude and geometry of SF3 and SF4. The reflections show subparallel and hummocky or undulated stratal patterns. B) The instantaneous phase profiles of two facies showing the lateral continuity and nature of reflection terminations against the upper and lower surfaces. C) Variance attribute illustrates the discontinuities along SF3 and SF4 caused by chaotic reflections.

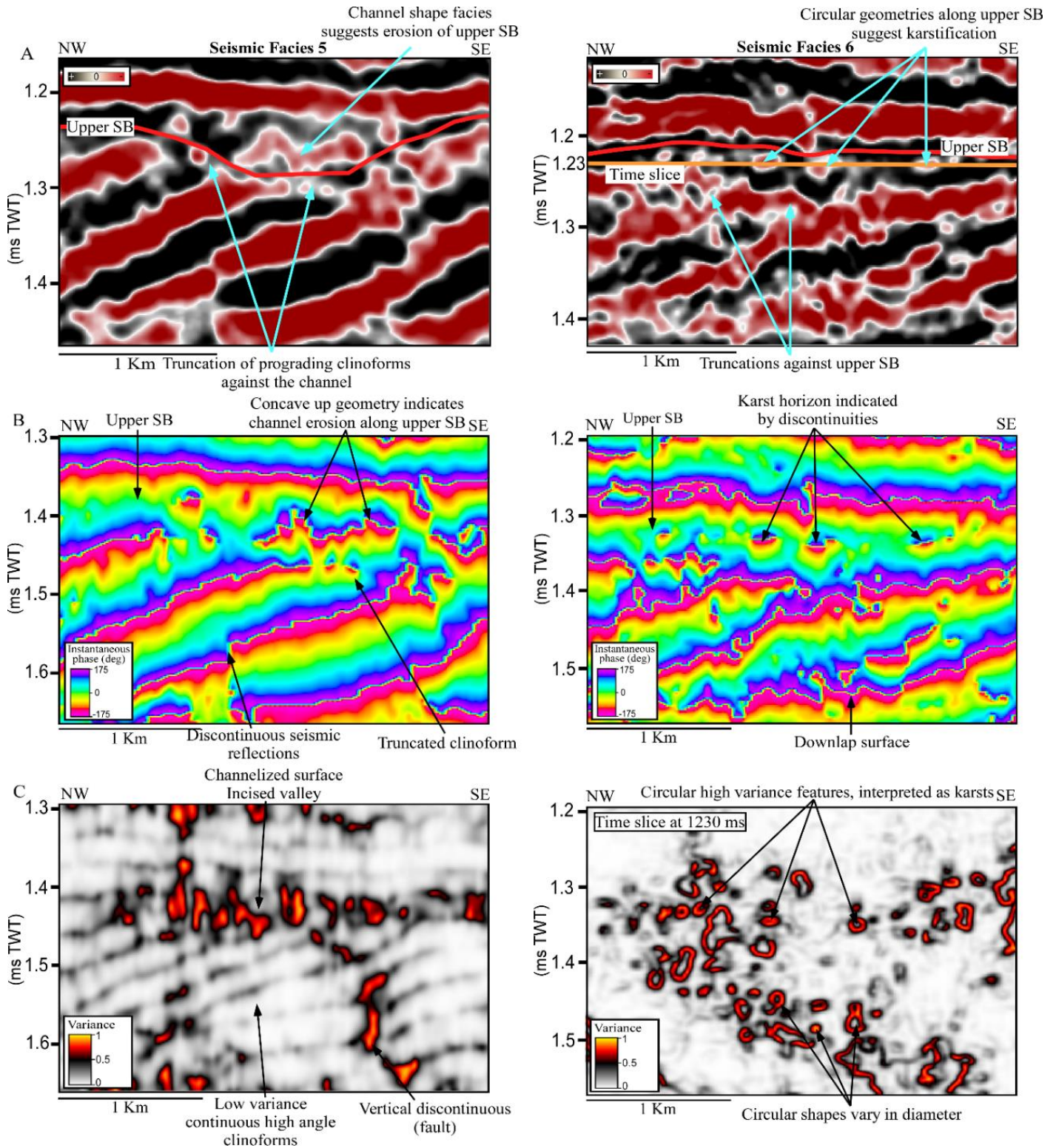


Fig. 7. Seismic vertical sections showing the amplitude and geometry of SF5 and SF6. The reflections show channel shape and broken reflection stratal patterns. B) The instantaneous phase profiles of two facies showing the discontinuities and nature of reflection terminations against the upper and lower surfaces. C) Variance time slice at 1230 ms illustrates the discontinuities along SF5 and SF6 caused by chaotic reflections and karst erosion.

4.4.1.2. Distal slope

The declivity of the distal slope varies from one place to another along the clinoform interval. The seismic facies of the distal slope consist of subparallel to chaotic and semi-continuous to continuous reflections of moderate amplitude. The reflections become more chaotic and less inclined basin ward. The distal slope clinoforms terminate against the upper surface in two areas along the platform. They extend laterally into the basin and become nearly horizontal (Fig. 4A). Their overall morphology suggests that they are possibly mass transport deposits, in which sediments are eroded

from platform top and margin, transported downslope by gravity induced flows, and redeposited along the lower slope, toe of slope, and basin. Well A2, which penetrates through the nearly horizontal clinoforms basin ward, also shows a serrated wireline log motif, but is distinctly different in its high GR readings (Fig. 4B). This Well shows that the distal slope facie is comprised of thick limestone successions with more shale units compared to the proximal slope (Fig. 4B). The log pattern along the distal slope is generally serrated, but a few tens of meters of funnel pattern cycles are also present. The irregular serrated log pattern may represent the deposits in the lower and deep marine slopes (Emery and Myers, 1996).

However, due to limitation of wireline log and core data, other depositional systems in the studied sequence are difficult to recognize and delineate, hence, only two depositional subsystems are emphasized in this study.

5. Conclusions

The internal geometry and depositional system of a Middle Eocene prograding clinoforms within the continental rift Sirt Basin were interpreted using wireline logs and 3-D seismic reflection profiles. This work reached the following conclusions:

1. The prograding clinoforms are bounded by a downlap surface at the base and by a truncational surface at the top.
2. Six seismic facies were identified based on seismic facies and attribute analyses (SF1 to SF6). The seismic facies show different geometries and indicate complex lithology and depositional systems. SF1 and SF2 that developed in the proximal area show progradational pattern on seismic section and wireline

logs. SF3 formed basinward of SF1 and SF2 and shows subparallel pattern on seismic section and serrated log motif. SF4 developed below the clinoform complex and displays hummocky internal configuration and was interpreted as a basin floor fan. SF5 is a channel-shaped facies formed on top of the proximal clinoforms and was interpreted as an incised valley. SF6 is seen as broken reflections on vertical seismic sections and as circular features on time slices. SF6 was interpreted as karst features developed on top of the clinoforms.

3. Two depositional systems were delineated: a proximal slope characterized by a sigmoidal and oblique parallel seismic pattern and by a funnel log trend, and a distal slope characterized by a subparallel seismic reflections and serrated log motif.
4. Seismic facies and attribute analyses have proved to be a highly effective method for delineating carbonate facies and depositional systems.

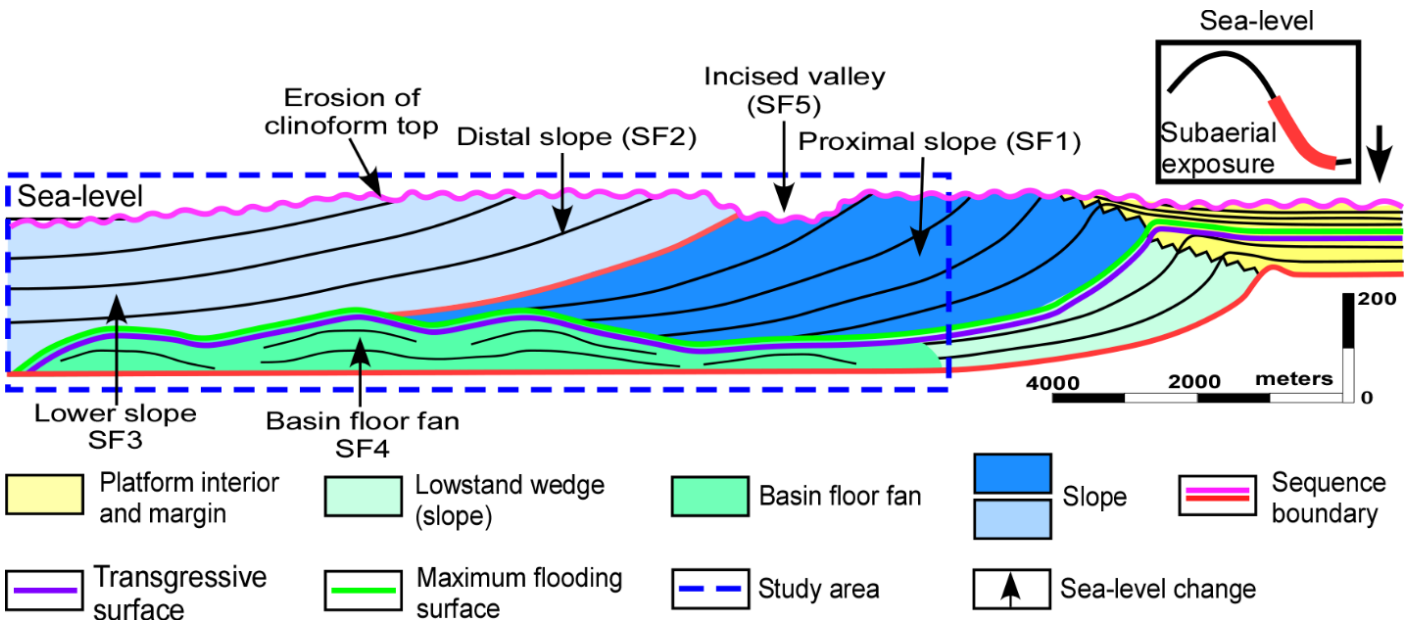


Fig.8. Schematic model of the studied clinoforms during its subaerial exposure showing the interpreted depositional system based on the seismic facies and attribute analyses. The seismic facies and attribute analysis, and the log facies and their stacking patterns enabled the subdivision of slope system into two different subsystems: proximal slope shown in blue and located close to the platform top and margin and distal slope outlined in light blue and located basinward of the proximal slope. The two subsystems are named on their position along the slope profile. The identified seismic facies and stratigraphic surfaces are shown on the model. The study area is outlined by the dashed blue box, and the section on the right is a speculation of the initial platform.

Acknowledgements

Wethank the Libyan National Oil Corporation (NOC) for providing the data used in this study and permission to publish the research results. We also thank Omar Al-Mukhtar University (OMU) for providing the soft wares and machines used in this research.

References

Abadi, A.M., Van Wees, J.D., Van Dijk, P.M. and Cloetingh, S.A. (2008) 'Tectonics and subsidence evolution of the Sirt Basin, Libya', *AAPG bulletin*, 92(8), pp. 993-1027.

Abdalla, M.A. (2021a) 'Seismic attributes aided detection of NW-SE trending faults developed on an isolated carbonate platform in the NW Sirte Basin, north central LIBYA', *International Journal of Engineering Applied Sciences and Technology*, 5, 53, pp.

Abdalla, M. and Yang, W. (2021) 'Progradation of a middle Eocene carbonate slope system, Assamoud Field, Sirte Basin, north central Libya–Implications on the dynamics of lateral growth of isolated carbonate platforms', *Marine and Petroleum Geology*, 129, p.105119.

Abdalla, M.A. (2021b) 'Seismic Attributes Aided Characterization of Margin Backstepping and Advance along Isolated Carbonate

Sequences, Sirt Basin, Libya', *Al-Mukhtar Journal of Sciences*, 36(4), pp. 280-287.

Adams, E. W., Schlager, W., (2000) 'Basic type of Carbonate Platform to Basin Transitions on Seismic Data and in Outcrops 245 submarine slope curvature', *Journal of Sedimentary Research*, 70, pp. 814–828.

Ambrose, G. (2000) 'The geology and hydrocarbon habitat of the Sarir Sandstone, SE Sirte Basin', Libya. *Journal of Petroleum Geology*, 23(2), pp. 165-192.

Baird, W. D., Aburawi R. M., Bailey J. N. (1996) 'Geohistory and petroleum in the central Sirte Basin, in Salem M. J., Busrewil M. T., Misallati A. A., Sola M. A., eds., *The geology of the Sirte Basin: Amsterdam, Elsevier*', 3, pp. 3–56.

Barr, F. T., Weegar, A. A. (1972) *Stratigraphic Nomenclature of the Sirte Basin, Libya*. Petroleum Exploration Society of Libya, p. 1-179).

Brown, A. R., (2004) Interpretation of 3-D seismic data (6th Ed.) American Association of Petroleum Geology Memoir, pp. 42, 54.

Cook, H. E., & Mullins, H. T., (1983) Basin margin environment, in P. A. Scholle, D. G. Bebout, and C. H. Moore, eds., *Carbonate depositional environments: AAPG Memoir 33*, pp. 540–617.

- Eberli, G. P., Anselmetti, F. S., Betzler, C., Van Konijnenburg, J. H., & Bernoulli, D. (2004) Carbonate platform to basin transitions on seismic data and in outcrops: Great Bahama Bank and the Maïella platform margin, Italy.
- Emery, D. and Myers, K. J. (1996) *Sequence Stratigraphy*. Victoria, Australia: Blackwell Science Ltd., p. 291.
- Gras, R., Thusu, B. (1998) 'Trap architecture of the early Cretaceous Sarir Sandstone in the eastern Sirte Basin, Libya', *Geological Society, London, Special Publications*, 132(1), pp. 317-334.
- Guiraud, R., Bosworth, W. (1997) 'Senonian basin inversion and rejuvenation of rifting in Africa and Arabia: synthesis and implications to plate-scale tectonics', *Tectonophysics*, 282(1-4), pp. 39-82.
- Hallett, D., Clark-Lowes, D. (2017) *Petroleum geology of Libya*. Elsevier, (<https://shop.elsevier.com/books/petroleum-geology-of-libya/hallett/978-0-444-63517-4>)
- Hart, B. S., (2012) Introduction to Seismic Interpretation. American Association of Petroleum Geology Discovery Series No. 16 (electronic book).
- Hine, A.C., Locker, S.D., Tedesco, L.P., Mullins, H.T., Hallock, P., Belknap, D.F., Gonzales, J.L., Neumann, A.C. and Snyder, S.W. (1992) 'Megabreccia shedding from modern, low-relief carbonate platforms, Nicaraguan Rise', *Geological Society of America Bulletin*, 104(8), pp. 928-943.
- Kenter, J. A. M., (1990) 'Carbonate platform flanks: Slope angle and sediment fabric', *Sedimentology*, 37, pp. 777-794.
- Koson, S., Chenrai, P. and Choowong, M. (2013) 'Seismic attributes and their applications in seismic geomorphology', *Bulletin of Earth Sciences of Thailand*, 6(1), pp. 1-9.
- Lemnifi, A. A., Liu, K. H., Gao, S. S., Reed, C. A., Elsheikh, A. A., Yu, Y., Elmelade, A. A. (2015) 'Azimuthal anisotropy beneath north central Africa from shear wave splitting analyses', *Geochemistry, Geophysics, Geosystems*, 16, pp. 1105-1114. <https://doi.org/10.1002/2014GC005706>.
- Lemnifi, A., Elshaafi, A., Browning, J., El Ebadi, S., Gudmundsson, A. (2017a) 'Crustal thickness beneath Libya and the origin of partial melt beneath AS Sawda Volcanic Province from receiver-function constraints', *J. Geophys. Res. Solid Earth*. <https://doi.org/10.1002/2017JB014291>
- Macurda Jr, D. B. (1997) 'Carbonate seismic facies analysis Carbonate seismology', *Society of Exploration Geophysicists Geophysical Developments Series*, 6, pp. 95-119.
- Mitchum Jr., R.M., Vail, P.R., Thompson III, S., (1977) Seismic stratigraphy and global changes of sea level; Part 2, the depositional sequence as a basic unit for stratigraphic analysis. In: Payton, C.E. (Ed.), *Seismic Stratigraphy; Applications to Hydrocarbon Exploration*, vol. 26. American Association of Petroleum Geologists Memoir, pp. 53-62.
- Mouzoughi, A. J. and Taleb, T. M. (1981) Tectonic elements of Libya, 1:2,000,000. National Oil Corporation, Libya.
- Roohi, M., (1996) Geological view of source-reservoir relationships in the western Sirte Basin. In: Salem, M.J., El-Hawat, A.S. and Sbeta, A.M., (eds), *The Geology of the Sirte Basin*, volume II. Elsevier, Amsterdam, p. 323-336.
- Sheriff, R. E., (2002) *Encyclopedic Dictionary of Applied Geophysics* (4th ed.), Society of Exploration Geophysicists, p. 429.
- Van der Meer, F. D., CLOETHING, S. (1993) 'Late Cretaceous and Tertiary subsidence history of the Sirte Basin (Libya); an example of the use of backstripping analysis', *ITC Journal*, (1), pp. 68-76.
- Wenneker, J.H.N., Wallace, K.F., Abugares, I.Y., (1996) The geology and hydrocarbons of the Sirte Basin: a synopsis. In: Salem, M.J., Mouzoughi, A.J., Hammuda, O.S. (Eds.), *The Geology of the Sirte Basin*, vol. 1. Elsevier, Amsterdam, pp. 3-56.